Thickness-Dependent Excitonic Properties of $WSe_2/FePS_3$ van der Waals Heterostructures

Xu Zhang[a, #], Chunli Wang[a, #], Zhenwei Ou[b, #], Xiaohong Jiang[c, d, #], Jinlian Chen[a], Huifang Ma[a], Chenyang Zha[a], Wei Wang[a], Linghai Zhang[a, *], Ti Wang[b, *], Lin Wang[a, *]

[a.] School of Flexible Electronics (Future Technologies) & Institute of Advanced Materials (IAM), Key Laboratory of Flexible Electronics (KLOFE), Jiangsu National Synergetic Innovation Center for Advanced Materials (SICAM), Nanjing Tech University (NanjingTech), Nanjing 211816, China

[b.] School of Physics and Technology, and Key Laboratory of Artificial Micro- and Nano-structures of Ministry of Education Wuhan University Wuhan 430072, China

[c.] MIIT Key Laboratory of Flexible Electronics (KLOFE), Shanxi Key Laboratory of Flexible Electronics (KLOFE), Xi'an Key Laboratory of Flexible Electronics (KLOFE), Xi'an Key Laboratory of Biomedical Materials & Engineering, Xi'an Institute of Flexible Electronics, Institute of Flexible Electronics (IFE), Northwestern Polytechnical University, Xi'an 710072, Shaanxi, China

[d.] Shaanxi Provincial Key Laboratory of Papermaking Technology and Specialty Paper Development, College of Bioresource Chemical and Materials Engineering, Shaanxi University of Science & Technology, Xi'an 710021, P. R. China

[#] These authors contributed equally to this work.

* Corresponding author.

E-mail: iam.lzhang@njtech.edu.cn

E-mail: wangti@whu.edu.cn

E-mail: iamlwang@njtech.edu.cn

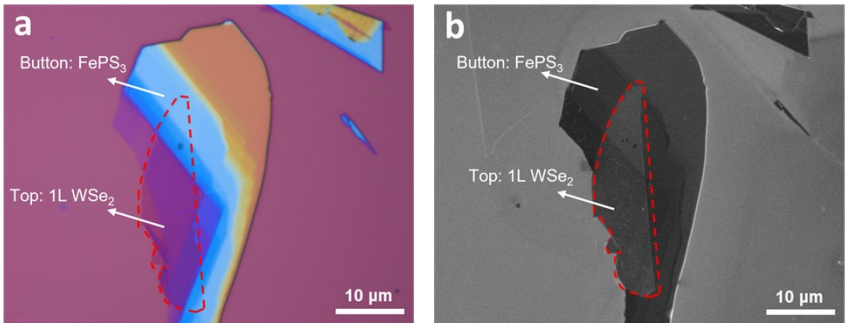

Figure S1 (a, b) The optical microscopy (OM) image and the corresponding scanning electron microscope (SEM) image of $WSe_2/FePS_3$ van der Waals heterostructures, respectively.

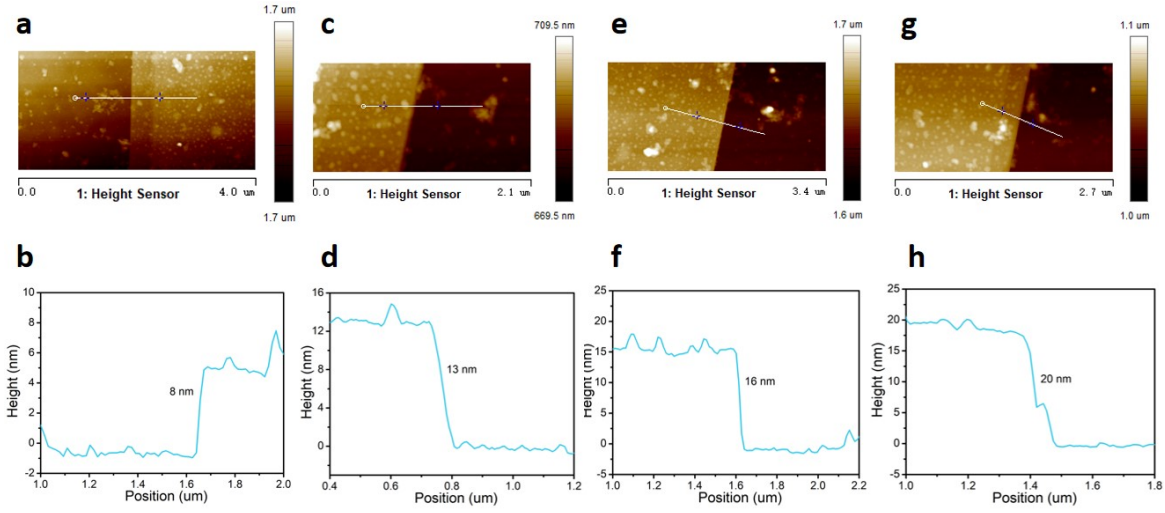

Figure S2. The atomic force microscope measurements of $WSe_2/FePS_3$ van der Waals heterostructures.

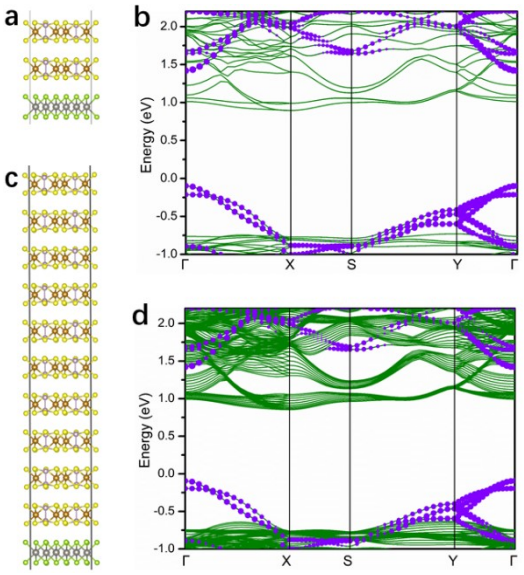

Figure S3. The relaxed structures of the monolayer-WSe_2/2L-$FePS_3$ (a) and monolayer-WSe_2/10L-$FePS_3$ (c) heterostructures. The band structures of the monolayer-WSe_2/2L-$FePS_3$ (b) and monolayer-WSe_2/10L-$FePS_3$ (d) heterostructures. The green lines are the energy bands of multilayered $FePS_3$ and the green lines with purple dots are the energy bands of monolayer-WSe_2.

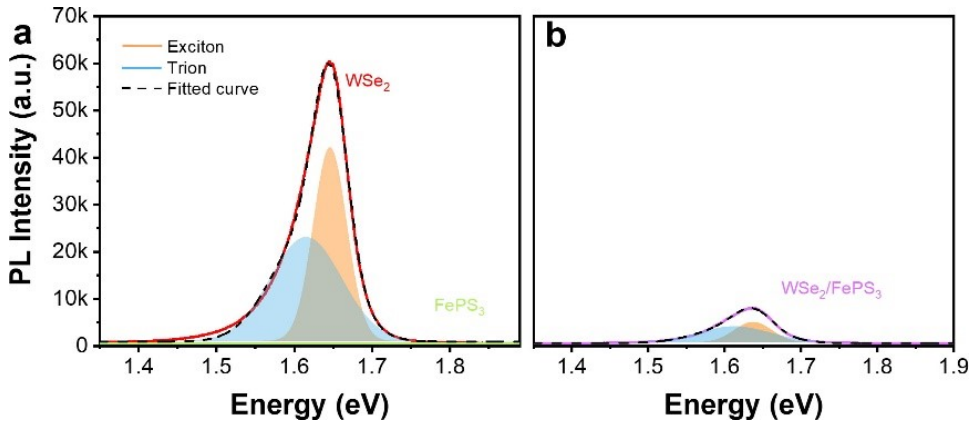

Figure S4. The PL spectra of isolated WSe_2 monolayer and isolated $FePS_3$ (a) as well as WSe_2/$FePS_3$ heterostructure (b) with fitted curves under the excitation of 532 nm at room temperature.

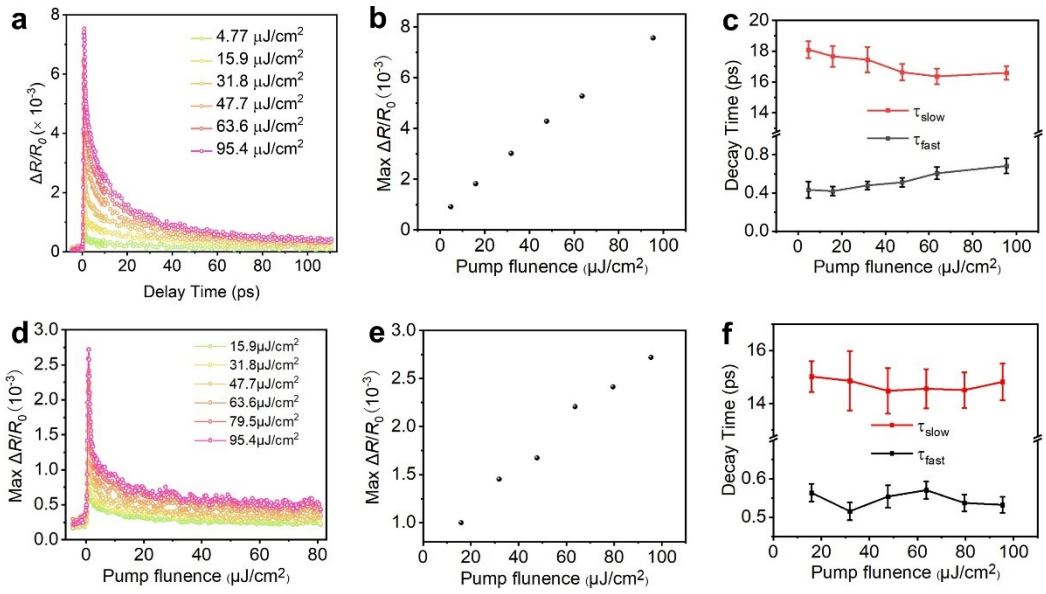

Figure S5. Photocarrier dynamics in individual monolayer WSe_2 and WSe_2/nL-$FePS_3$ heterostructures. (a, d) Differential reflection signals of WSe_2 monolayer and WSe_2/nL-$FePS_3$ heterostructures as a function of the probe delay measured with a 400 nm pump and a 743 nm probe under various excitation fluence as indicated, respectively. (b, e) Peak differential reflection signal of WSe_2 monolayer and WSe_2/nL-$FePS_3$ heterostructures as a function of the excitation fluence, respectively. (c, f) Two time constants deduced from biexponential fits of WSe_2 monolayer and WSe_2/nL-$FePS_3$ heterostructures as a function of the excitation fluence, respectively.

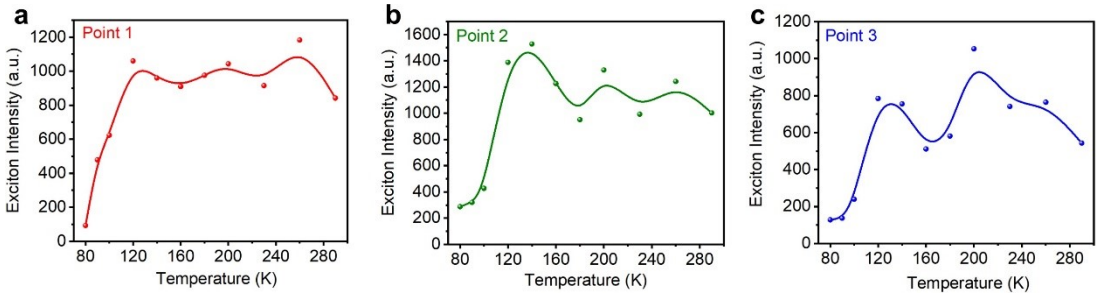

Figure S6. (a-c) The neutral exciton intensity of point 1, point 2, point 3 of WSe_2/nL-$FePS_3$ heterostructure as a function of temperature under 532 nm excitation with the power density of 9.55 mJ/cm^2, respectively.